Bio-Mimetic Trajectory Generation of Robots via Artificial Potential Field With Time Base Generator

Toshio Tsuji, *Member, IEEE*, Yoshiyuki Tanaka, Pietro G. Morasso, Vittorio Sanguineti, and Makoto Kaneko, *Senior Member, IEEE*

***Abstract*—This paper proposes a new trajectory generation method that allows full control of transient behavior, namely, time-to-target and velocity profile, based on the artificial potential field approach for a real-time motion planning problem of robots. Little attention, in fact, has been paid to the temporal aspects of this class of path planning methods. The ability to control the motion time to the target as well as the velocity profile of the generated trajectories, however, is of great interest in real-life applications. In the paper, we argue that such transient behavior should be taken into account within the framework of the artificial potential field approach.**

***Index Terms*—Artificial potential field, human-like movements, time base generator, trajectory generation.**

I. Introduction

REMARKABLE developments of human-shaped robots have been achieved with the latest progress of robotic technology in recent years [1], [2], so that a friendly feeling of a human toward the robot is practically realized from a cosmetic point of view. It has been expected that the robots will be able to cowork and coexsit with a human at home or a workspace in the near future. However, no matter how similar to a human being in appearance the robot is, it is very difficult to cowork with a human in daily activities if it cannot act or perform a task with human-like movements.

The purpose of the present paper is to develop a method for generating a bio-mimetic trajectory of robots which has characteristics of human movements by introducing the mechanism of human hand trajectory generation into the Artificial Potential Field Approach (APFA) [3]–[13] which has been often used for the trajectory planning of the robots. The final goal of this study is to control the robot with human-like smooth movements.

In the APFA, a target position is represented by an artificial attractive potential field and obstacles by corresponding repulsive fields, so that the trajectory to the target can be associated with the unique flow-line of the gradient field through the initial position and can be generated via a flow-line tracking process. This approach is suitable for real-time motion planning of robots since the algorithm is simple and computationally much less expensive than other methods based on global information about the task space. However, at least two important weak points should be singled out: local minima and transient control.

With regard to the first problem, it is a simple observation that when the attractive potential to the goal and the repulsive one from the obstacles are equal, the gradient vector of the potential field becomes zero and the robot falls into a *deadlock*. Many methods have been proposed to overcome this problem. Connolly, Burns and Weiss [5] proposed a method using Laplace's differential equation based on the idea that the deadlock problem is completely solved when one can define a potential function which does not include local minima structurally. In fact, some potential functions of this kind have been proposed [6]–[8].

The other disadvantage is that it is difficult in the artificial potential field framework to regulate the transient behavior of the generated trajectories such as the movement time to the target and the shape of the velocity profile. For example, even if the potential function without local minima is used, it is difficult to estimate the movement time required for reaching beforehand. Moreover, the velocity profile of the generated trajectory cannot be adjusted as required since it is determined by the shape of the potential field. Hence, although one of the most crucial winning features of the APFA is real-time applicability, it is difficult to use the generated trajectory for the control of the robots in real time. Quite likely, the scarce consideration about the transient behavior of the planned paths was motivated by the fact that the deadlock-free requirement was the overwhelming concern in the field. For this problem, there have been some studies on the time-optimal trajectory planning to the target [8]–[10]. In these studies, the movement time is regulated by using the spatial trajectory, generated beforehand, as a parameter. Therefore, whenever the space trajectory is renewed by changing the task space condition, the planning of the movement time has to be redone. Also, the previous studies do not consider regulation of the velocity profile to reach the target point.

Recently, Morasso *et al.* [14], [15] proposed a two-dimensional trajectory generation approach for modeling human reaching movements. In this method, the hand trajectory is generated by synchronizing the translational and rotational velocities of the hand with a scalar signal generated by a time base generator (TBG). The TBG generates a time-series signal, which is a scalar signal with a controllable finite duration and bell-shaped velocity profile. Thus, the movement time and the velocity profile of the hand trajectory can be regulated indirectly by adjusting the parameters of the TBG. Then, Tsuji *et al.* [16]–[19] applied the TBG mechanism to the control of the robots.

Manuscript received February 6, 1999; revised August 17, 2000.

T. Tsuji, Y. Tanaka, and M. Kaneko are with the Department of Artificial Complex Systems Engineering, Graduate School of Engineering, Hiroshima University, Higashi-Hiroshima, 739-8527 Japan (e-mail: tsuji@hfl.hiroshima-u.ac.jp; ytanaka@hfl.hiroshima-u.ac.jp; kaneko@hfl.hiroshima-u.ac.jp).

P. G. Morasso and V. Sanguineti are with the Department of Informatics, Systems and Telecommunications (DIST), University of Genova, I-16145 Genova, Italy (e-mail: morasso@dist.unige.it; sangui@dist.unige.it).

Digital Object Identifier 10.1109/TSMCC.2002.807273

In this paper, a new trajectory generation method is proposed by introducing the TBG into the APFA. The method can regulate the movement time from the initial position to the goal and the velocity profile of the robot, in which the generating trajectory has the characteristics of human-like movements; i.e., the velocity profile is bell-shaped. Remarkably, the method can take advantage of a variety of potential functions developed by people working in the field (particularly, the functions which are deadlock-free), because it is a property of the proposed mechanism that the temporal structure of the planned path is regulated through the TBG and is rather independent of the specific type of potential function.

The paper is organized as follows: Section II describes the APFA and points out its general problem. In Section III, the basic principles of the proposed method, including examples of the TBG's, are explained. Then the method is applied to a multi-joint redundant manipulator and a unicycle-like vehicle in Section IV and Section V, respectively. It is shown from computer simulations that the method can regulate in a smooth way the spatio-temporal structure of the trajectories.

II. Artificial Potential Field Approach

Let us consider the following dynamic linear system with a drift part:

$$\frac{d}{dt}X = PX + QF_X \tag{1}$$

where

$$P = \begin{bmatrix} 0_{n+n} & I_{n+n} \\ 0_{n+n} & 0_{n+n} \end{bmatrix},\ Q = \begin{bmatrix} 0_{n+n} \\ I_{n+n} \end{bmatrix}.$$

$X = [x_1, \ldots, x_n, \dot{x}_1, \ldots, \dot{x}_n]^T = [x^T, \dot{x}^T]^T \in \Re^{2n}$ is the state variable vector, $F_X \in \Re^n$ is the input vector, $0_{n+n} \in \Re^{n\times n}$ is the zero matrix and $I_{n+n} \in \Re^{n\times n}$ is the unit matrix. In this section, in order to clarify the purpose of this study, we attempt to design the feedback control law F_X to stabilize the system (1) toward the equilibrium point $X = 0$ by using the artificial potential field approach (APFA).

The potential function with quadratic form V_X can be defined when the target is set at $X = 0$ as

$$V_X = \sum_{i=1}^{n} \frac{1}{2}\left(k_i x_i^2 + k_{n+i}\dot{x}_i^2\right) = \frac{1}{2}X^T K_a X \tag{2}$$

where $K_a = \text{diag.}(k_1, k_2, \ldots, k_{2n})$ under $k_i > 0$ $(i = 1, \ldots, 2n)$. Based on the potential function defined by (2), a feedback control law which stabilizes the system asymptotically can be designed as

$$F_X = -K_b X \tag{3}$$

where

$$K_b = \left[\begin{array}{cccc|c} \frac{k_1}{k_{n+1}} & 0 & \cdots & 0 & \\ 0 & \frac{k_2}{k_{n+2}} & \cdots & 0 & \\ \vdots & \vdots & \ddots & \vdots & I_{n+n} \\ 0 & 0 & \cdots & \frac{k_n}{k_{2n}} & \end{array}\right].$$

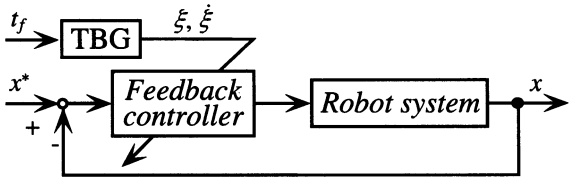

Fig. 1. Block diagram of the proposed control system.

Substituting the designed controller F_X given in (3) into the time derivation of the potential function $\dot{V}_X$ yields

$$\dot{V}_X = -X^T K_c X \le 0 \tag{4}$$

where

$$K_c = \text{diag.}\,(0, 0, \ldots, 0, k_n, k_{n+1}, \ldots, k_{2n}).$$

The potential function V_X given in (2) does not have any local minimum so that $F_X = 0$ except at the equilibrium point $X = 0$ and has the minimum value $V_X = 0$ at $X = 0$. Thus, V_X is controlled to the equilibrium point by means of the feedback control law F_X given in (3). Moreover, substituting (3) into (1) the following linear system can be derived:

$$\ddot{x} + \dot{x} + K_d x = 0 \tag{5}$$

where

$$K_d = \text{diag.}\left(\frac{k_1}{k_{n+1}}, \frac{k_2}{k_{n+2}}, \ldots, \frac{k_n}{k_{2n}}\right).$$

Obviously, the system given in (1) is asymptotically stable under the designed feedback controller F_X. However, it can be concluded that it is impossible to regulate the convergence time and the dynamic behavior of the system as hoped [18].

III. Trajectory Generation Method Using Time Base Generator

In this section, the proposed method based on the APFA with the TBG [16]–[19] and the time scale transformation [21] is explained in detail.

Fig. 1 shows a block diagram of the proposed control system, where x^* is a target point. The TBG generates a nonincreasing function $\xi(t)$ with a bell-shaped velocity profile satisfying $\xi(0) = 1$ and $\xi(t_f) = 0$.

A. TBG

The TBG was originally defined for a model of human movements [14], [15]. Morasso *et al.* derived the TBG with a bell-shaped velocity profile in order to represent the feature of the end-point trajectory.

In order to illustrate the operation of the TBG in the control loop, the *terminal attractor concept* is used. This special kind of attractor was introduced by Zak [20] into a nonlinear neural network model and it was shown that a system with a terminal attractor always converges to the equilibrium point in a finite time, where the sufficient condition to have the terminal attractor is that the Lipschitz condition of ordinary differential equations is violated at the equilibrium point.

The dynamics of the TBG is defined as follows:

$$\dot{\xi} = \phi(\xi) = -\gamma(\xi(1-\xi))^{\beta} \tag{6}$$

where γ is a positive constant which allows control of the convergence time t_f and β is a constant which determines the behavior of the TBG, with $0 < \beta < 1.0$. From (6) it can be seen that ξ has two equilibrium points: a stable one ($\xi = 0$) and an unstable one ($\xi = 1$). Consequently, ξ always converges stably to $\xi = 0$, when an initial value of ξ is chosen as $\xi(0) = 1 - \epsilon$, with a very small positive constant ϵ. Then the convergence time t_f can be calculated as

$$t_f = \int_0^{t_f} dt \approx \int_1^0 \frac{d\xi}{\phi(\xi)} = \frac{\Gamma^2(1-\beta)}{\gamma\Gamma(2-2\beta)} \tag{7}$$

where $\Gamma(\cdot)$ is the gamma function (Euler's integral of the second kind). Thus, the system converges to the equilibrium point $\xi = 0$ in the finite time t_f if the parameter γ is chosen as

$$\gamma = \frac{\Gamma^2(1-\beta)}{t_f\Gamma(2-2\beta)}. \tag{8}$$

This means that the equilibrium point is a terminal attractor. The velocity signal $\dot{\xi}(t)$, which is null for $t = 0$ and $t = t_f$, has a bell-shaped profile with the maximum absolute value at $t = t_f/2$: $|\dot{\xi}(t_f/2)| = \gamma 4^{-\beta}$. With regard to the acceleration profile, the following form can be derived as

$$\frac{d^2\xi}{dt^2} = \gamma^2\beta(1-2\xi)\{\xi(1-\xi)\}^{2\beta-1} \tag{9}$$

and it can be seen that the condition for the existence of a bounded acceleration at the equilibrium point is given by the inequality $1/2 \le \beta < 1$. Then, the jerk of $\xi(t)$ is derived by differentiating (9)

$$\frac{d^3\xi}{dt^3} = -\gamma^3\beta\{(2\beta-1)(1-2\xi)^2 - 2\xi(1-\xi)\}\{\xi(1-\xi)\}^{3\beta-2} \tag{10}$$

which gives the following more restrictive condition for having a bounded jerk: $2/3 \le \beta < 1$. Figs. 2 and 3 show the changes of $\xi(t)$ generated by the TBG depending on the parameters t_f and β. In Fig. 2, the time histories of $\xi(t)$ and $\dot{\xi}(t)$ are shown depending on the convergence time $t_f = 1.0$, 1.5 and 2.0 [s] under the parameters $\beta = 0.5$ and $\epsilon = 1.0 \times 10^{-9}$. All trajectories converge to the equilibrium point at the specified time t_f. Moreover, Fig. 3 shows the time histories of $\xi(t)$ depending on the change of the power parameter $\beta = 0.25$, 0.5 and 0.75 with $t_f = 1.0$ [s] and $\epsilon = 1.0 \times 10^{-9}$. The time history of $\xi(t)$ can be regulated through the power parameter β while the convergence time remains constant.

In summary, by selecting two parameters of the TBG (t_f and β), a family of time-varying signals $\xi(t)$ can be generated. Note that, from the point of view of real-time implementation, it is possible to use any scalar function of time satisfying the properties of $\xi(t)$ described above: half period of the cosine function, a look-up table etc.

B. Control Law With the TBG Based Method

The basic idea of the proposed method is to compress a time scale of the controlled system with the TBG according to the specified convergence time t_f in the actual time scale and to design the asymptotic stabilizer for the time scaled system by means of the APFA.

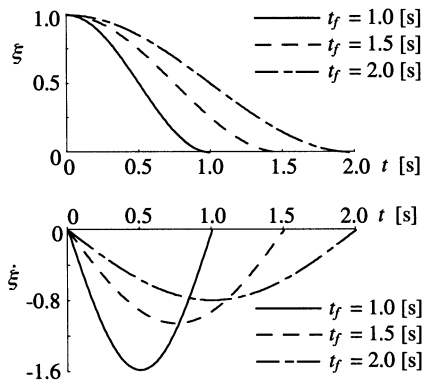

Fig. 2. Change of $\xi(t)$ depending on the convergence time t_f with the constant power parameter $\beta = 0.5$.

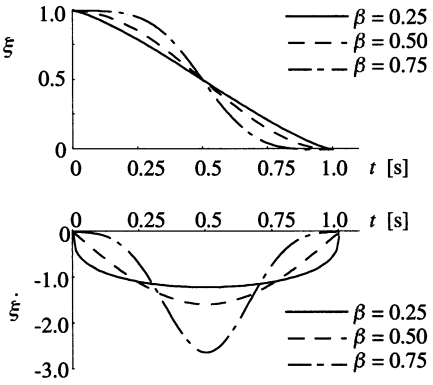

Fig. 3. Change of $\xi(t)$ depending on the power parameter β with the constant convergence time $t_f = 1.0$ [s].

The time scale compression with the TBG can be realized by the time scale transformation [21] with the virtual time scale whose infinite time corresponds to a specified finite time t_f of the TBG in the actual time scale. Then, the relationship between actual time t and virtual time s is given by

$$\frac{ds}{dt} = a(t) \tag{11}$$

where the continuous function $a(t)$ is called a time scale function [21]. In order to compress the time scale of the system with the TBG, the time scale function $a(t)$ is defined as

$$a(t) = -p\frac{\dot{\xi}}{\xi} \tag{12}$$

where p is a positive constant. From (11) and (12), the virtual time s can be represented with respect to ξ as follows:

$$s = \int_0^t a(t)dt = -p\ln\xi(t). \tag{13}$$

The parameter p can regulate the transformation of the time axis. The compressibility of the time axis becomes larger near the specified time as p decreasing, while it becomes uniform in all the time as p increasing. Generally, the stability and dynamic property of systems do not change in any time scale when a

strictly monotone increasing function with respect to the actual time is used as the time scale function. It is obvious that virtual time s given in (13) never goes backward against actual time t, so that virtual time s is used as a new time scale in time scale transformation of the original system (1) in order to derive the proposed controller.

The system given in (1) can be rewritten in the virtual time scale s as

$$\frac{d}{ds}X = \frac{dX}{dt}\frac{dt}{ds} = \frac{1}{a(t)}\dot{X}. \tag{14}$$

Applying the state and input transformation with the new state variable Ψ and the new input F_Ψ, defined as

$$\begin{aligned}\Psi =& [\psi_1, \ldots, \psi_n, \psi_{n+1}, \ldots, \psi_{2n}]^T \\ =& \left[x^T, \frac{\dot{x}^T}{a(t)}\right]^T \end{aligned} \tag{15}$$

$$F_\Psi = \frac{d}{ds}\left(\frac{1}{a(t)}\right)\dot{x} + \frac{1}{a^2(t)}F_X \tag{16}$$

to the system (14), the new linear system in the transformed time scale is obtained as follows:

$$\frac{d}{ds}\Psi = P\Psi + QF_\Psi. \tag{17}$$

The next step is to design the feedback control law which can stabilize this time scaled system (17) asymptotically in the virtual time scale by means of the conventional APFA. The potential function with quadratic form V_Ψ for the time scaled system (17) can be defined as follows:

$$\begin{aligned}V_\Psi =& \sum_{i=1}^{n} V_{\psi_i} = \sum_{i=1}^{n} \frac{1}{2}\left(k_i\psi_i^2 + k_{n+i}\psi_{n+i}^2\right) \\ =& \frac{1}{2}\Psi^T K_a \Psi. \end{aligned} \tag{18}$$

Designing the feedback control law F_Ψ based on V_Ψ with the APFA as

$$F_\Psi = -K_b\Psi \tag{19}$$

the time-derivative of the potential function in the new time scale yields

$$\frac{d}{ds}V_\Psi = -\Psi^T K_c \Psi \leq 0. \tag{20}$$

The time scaled system is stabilized asymptotically in the virtual time scale by means of the designed feedback controller F_Ψ given in (19).

By inverse time scale transformation from virtual time s to actual time t for the designed stabilizer F_Ψ with (15) and (16), the following feedback control law F_X for the original system (1) can be obtained as

$$F_X = -a^2(t)K_d x - \left(a(t) - \frac{\dot{a}(t)}{a(t)}\right)\dot{x}. \tag{21}$$

The infinite time in the virtual time scale is corresponding to the finite time t_f in the actual time scale. Therefore, the inverse time scale transformation for the feedback controller F_Ψ can be considered as the compression of the virtual time scale. This implies that the state variable Ψ is converged to zero by the feedback control law F_X given in (21) at the specified time t_f.

Substituting the feedback control law F_X into the original linear system equation given in (1), the following second-order differential equation can be obtained:

$$\ddot{x} = -p^2\left(\frac{\dot{\xi}}{\xi}\right)^2 K_d x + \left\{(p-1)\left(\frac{\dot{\xi}}{\xi}\right) + \left(\frac{\ddot{\xi}}{\dot{\xi}}\right)\right\}\dot{x}. \tag{22}$$

From (22), Euler's equation with respect to x and ξ can be derived as

$$\xi^2\frac{d^2x}{d\xi^2} - (p-1)\xi\frac{dx}{d\xi} + K_d p^2 x = 0. \tag{23}$$

Since the nonincreasing function ξ converges to zero at finite time t_f, the necessary and sufficient condition to converge x_i, $\dot{x}_i$ and $\ddot{x}_i$ to zero at the specified time t_f is given depending on the discriminant of the characteristic polynomial of (23) $D_{x_i} = 4k_i/k_{n+i} - 1$ as follows (see Appendix A):

$$\begin{aligned}&(1)\ \text{if } D_{x_i} \geq 0 \text{ then p} > 4(1-\beta), \\ &(2)\ \text{if } -1 < D_{x_i} < 0 \text{ then p} > \frac{4(1-\beta)}{1 - j\sqrt{D_{x_i}}}\end{aligned}$$

where $j^2 = -1$. Then, with the controller F_X, each element of the potential function V_{Ψ_i} reached zero at t_f in the actual time scale (see Appendix B).

Thus, it can be concluded that the feedback control law F_X (21) designed by the proposed method can regulate the dynamic behavior of the robot and the convergence time to reach the goal. Since the maximum torque until the robot reaches the goal position can be computed with the TBG dynamics beforehand, it is also possible to cope with the torque limited problem by adjusting the movement time to the goal.

IV. Trajectory Generation of a Multi-Joint Redundant Manipulator

A redundant manipulator which possesses extra degrees of freedom to execute a given task has a desirable feature that may lead to more dexterity and versatility of robot motions. Research activities on the resolution of redundancy have been increased in terms of how to determine a manipulator configuration that is constrained to generate a specified end-effector trajectory from the initial position to the target position x^* by optimizing various secondary criteria such as singularity avoidance, obstacle avoidance and various measures of dexterity [22]–[25]. On the other hand, a force/torque relationship of the manipulator has been pointed out by Khatib [26]. He pioneered the use of the null space on the force/torque transformation in order to control the internal joint motion of the redundant manipulator. In this section, the general approach described in the previous section is applied to the on-line spatio-temporal path planning problem of the end-effector with significant advantages of redundancy by utilizing the force/torque relationship.

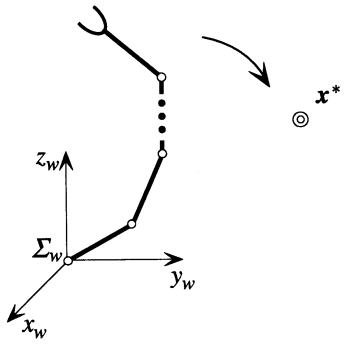

Fig. 4. An n-joint redundant manipulator.

A. Dynamics of Redundant Manipulators

The joint space motion equation of an n degree-of-freedom manipulator whose end-effector is operating in the m dimensional task space, as shown in Fig. 4, can be expressed as

$$M(q)\ddot{q} + h(q,\dot{q}) + g(q) = \tau \tag{24}$$

where $q \in \Re^n$ is the joint angle vector; $M(q) \in \Re^{n\times n}$ is the nonsingular inertia matrix; $h(q,\dot{q}) \in \Re^n$ is the nonlinear term including the joint torque due to the Coliolies and centrifugal force; $g(q) \in \Re^n$ is the joint torque due to gravity; and $\tau \in \Re^n$ is the joint torque vector. On the other hand, the dynamics of the end-effector can be written in the operational space as [26]

$$M_x(q)\ddot{x} + h_x(q,\dot{q}) + g_x(q) = F \tag{25}$$

where $x \in \Re^m$ is the current end-effector position; $F \in \Re^m$ is the end-effector force vector; $M_x(q) = (JM^{-1}(q)J^T)^{-1} \in \Re^{m\times m}$ is the operational space kinetic energy matrix; $J \in \Re^{m\times n}$ is the Jacobian matrix; and also

$$\begin{aligned} h_x(q,\dot{q}) =& \bar{J}^T h(q,\dot{q}) - M_x(q)\dot{J}\dot{q} \\ g_x(q) =& \bar{J}^T g(q) \\ \bar{J} =& \left(M_x(q)JM^{-1}(q)\right)^T. \end{aligned}$$

When a manipulator possesses extra degree-of-freedom to execute a given task, i.e., $m < n$, the joint torque of redundant manipulators can be decomposed into two elements: the joint torque $\tau_{effector} \in \Re^n$ to operate the end-effector and the joint torque $\tau_{joint} \in \Re^n$ to control the additional freedom of joint motion with redundancy of a manipulator. In this case, there exists the following force/torque relationship between the joint torque $\tau_{effector}$ and the operational force F:

$$\tau_{effector} = J^T F. \tag{26}$$

On the other hand, the joint torque τ_{joint} always satisfies the following condition given by

$$\bar{J}^T \tau_{joint} = 0. \tag{27}$$

This equation implies that the joint torque τ_{joint} must lay in the null space associated with the matrix $\bar{J}^T$ so as not to produce any acceleration at the end-effector. The general solution τ_{joint} for this condition given by

$$\tau_{joint} = G\tau^* \tag{28}$$

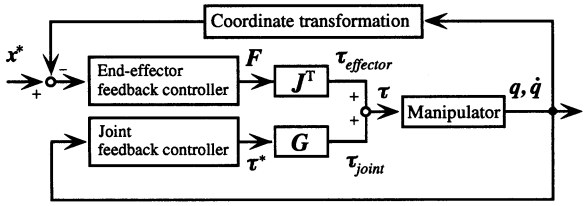

Fig. 5. Block diagram of the feedback control system for a redundant manipulator.

where τ^* is an arbitrary n dimensional vector; and $G = I - J^T\bar{J}^T \in \Re^{n\times n}$ defines the mapping to the null space associated with $\bar{J}^T$. Consequently, the total joint torque τ for a redundant manipulator can be recomposed from (26) and (28) as follows:

$$\begin{aligned} \tau =& \tau_{effector} + \tau_{joint} \\ =& J^T F + G\tau^*. \end{aligned} \tag{29}$$

In this paper, the feedback control law F for operating the end-effector to the target point x^* and τ^* for controlling additional freedom of motion of a manipulator are designed with the proposed method, respectively. The total joint torque composed of those designed controllers allows a redundant manipulator to perform a given task by utilizing arm redundancy efficiently. Fig. 5 shows the block diagram of this feedback system of the redundant manipulator.

B. Derivation of the TBG Built-In Controller

The two dynamic equations in the joint space (24) and in the operational space (25) can be rewritten into the following linear system with the state variable $Z = [x, q, \dot{x}, \dot{q}]^T$ as

$$\frac{d}{dt}Z = \begin{bmatrix} 0 & I \\ 0 & 0 \end{bmatrix} Z + \begin{bmatrix} 0 \\ I \end{bmatrix} \begin{bmatrix} F_t \\ \tau_t \end{bmatrix} \tag{30}$$

$$F_t = M_x^{-1}(q)\left\{F - (h_x(q,\dot{q}) + g_x(q))\right\} \tag{31}$$

$$\tau_t = M^{-1}(q)\left\{\tau - (h(q,\dot{q}) + g(q))\right\} \tag{32}$$

where $0 \in \Re^{(m+n)\times(m+n)}$ is the zero matrix and $I \in \Re^{(m+n)\times(m+n)}$ is the unit matrix.

The system given in (30) can be rewritten in the virtual time scale s as follows:

$$\frac{d}{ds}\Psi = \begin{bmatrix} 0 & I \\ 0 & 0 \end{bmatrix} \Psi + \begin{bmatrix} 0 \\ I \end{bmatrix} \begin{bmatrix} F_s \\ \tau_s \end{bmatrix} \tag{33}$$

where

$$\Psi = [\psi_1, \psi_2, \psi_3, \psi_4] = \left[x, q, \frac{\dot{x}}{a(t)}, \frac{\dot{q}}{a(t)}\right]^T \tag{34}$$

$$F_s = \frac{d}{ds}\left(\frac{1}{a(t)}\right)\dot{x} + \frac{1}{a^2(t)}F_t \tag{35}$$

$$\tau_s = \frac{d}{ds}\left(\frac{1}{a(t)}\right)\dot{q} + \frac{1}{a^2(t)}\tau_t. \tag{36}$$

As previously defined in the relationship between actual time and virtual time given in (13), stability of the time scaled system given in (33) is the same as the original system in the actual time [21]. Hence, there exists a feedback control law to stabilize the time scaled system asymptotically.

The potential function with quadratic form $V^{\psi}_{effector}$ for the control of the end-effector to the target position ψ_1^* in the virtual time scale can be defined as follows:

$$V^{\psi}_{effector} = \frac{1}{2}(\psi_1^* - \psi_1)^T K_1 (\psi_1^* - \psi_1) + \frac{1}{2}{\psi_3}^T K_2 \psi_3 \quad (37)$$

where $K_i = \text{diag.}(k_1^i, k_2^i, \ldots, k_m^i)$ under $k_m^i > 0\,(i = 1, 2)$. Designing the feedback control law F_s based on $V^{\psi}_{effector}$ as

$$F_s = -{K_2}^{-1}\{K_1(\psi_1 - \psi_1^*) + \psi_3\} \quad (38)$$

we have the time-derivative of the potential function $V^{\psi}_{effector}$ in the new time scale as follows:

$$\begin{aligned}\frac{d}{ds}V^{\psi}_{effector} &= {\psi_3}^T\left\{K_1(\psi_1 - \psi_1^*) + K_2\frac{d\psi_3}{ds}\right\} \\ &= -\|\psi_3\|^2 \le 0. \end{aligned} \quad (39)$$

By inverse transformation of time scale from the virtual time s to the actual time t for the controller F_s with (34) and (35), the controller F_t in the actual time is derived as

$$F_t = -a^2(t)K_2^{-1}K_1(x - x^*) - \left(a(t)K_2^{-1} - \frac{\dot{a}(t)}{a(t)}\right)\dot{x}. \quad (40)$$

From (31) and (40), the feedback control law F^{ψ} for control of the dynamic behavior of the end-effector can be obtained as follows:

$$F^{\psi} = M_x(q)F_t + h_x(q, \dot{q}) + g_x(q). \quad (41)$$

The end-effector of the manipulator is controlled to the target position at the convergence time t_f by means of the joint torque $\tau_{effector}$ equivalent to the feedback control law F^{ψ} given in (41). For a redundant manipulator, however, the joints may continue to move although the end-effector arrives at the target position since the designed controller F^{ψ} can not control the extra freedom of joint motion directly. For this problem, we utilize the null space on the force/torque transformation [26] to control the internal joint motion. Here, the potential function V^{ψ}_{joint} to derive the feedback controller τ_s in the virtual time s is defined as

$$V^{\psi}_{joint} = \frac{1}{2}{\psi_4}^T K_3 \psi_4 + \zeta(s)Q_s(\psi_2) \quad (42)$$

where $K_3 = \text{diag.}(k_1^3, k_2^3, \ldots, k_n^3)$ under $k_n^3 \ge 0$; $Q_s(\psi_2)$ is the differentiable potential function in the virtual time scale; and $\zeta(s)$ is a positive nonincreasing scalar function. The first term on the right side of (42) is used in order to dampen the redundant joint motion when the end-effector arrives at the goal and the second one is used to realize the desired posture of the manipulator ψ_2^* corresponding to the minimum of the potential function $Q_s(\psi_2)$. It should be noted that the potential function $Q_s(\psi_2)$ can be maximized under the negative nondecreasing coefficient function $\zeta(s)$. Differentiating the potential function $Q_s(\psi_2)$ with respect to virtual time s yields

$$\frac{\partial Q_s}{\partial s} = \left(\frac{\partial \psi_2}{\partial s}\right)^T \frac{\partial Q_s}{\partial \psi_2} = {\psi_4}^T \frac{\partial Q_s}{\partial \psi_2}. \quad (43)$$

With the new system (33) and the above (43), the time-derivative of the potential function V^{ψ}_{joint} in the virtual time s can be represented as

$$\frac{d}{ds}V^{\psi}_{joint} = {\psi_4}^T\left(K_3\tau_s + \zeta(s)\frac{\partial Q_s}{\partial \psi_2}\right) + \frac{d\zeta(s)}{ds}Q_s(\psi_2). \quad (44)$$

Designing the feedback controller τ_s with the nonincreasing scalar function $\zeta(s)$ in the new time scale as

$$\tau_s = -{K_3}^{-1}\left(\psi_4 + \zeta(s)\frac{\partial Q_s}{\partial \psi_2}\right) \quad (45)$$

we can have

$$\frac{d}{ds}V^{\psi}_{joint} = -\|\psi_4\|^2 + \frac{d\zeta(s)}{ds}Q_s(\psi_2) \le 0. \quad (46)$$

This indicates that the potential function V^{ψ}_{joint} is stabilized to the equilibrium point by means of the feedback controller τ_s in the virtual time scale.

Then, we define the nonincreasing function $\zeta(s)$ in the new time scale as

$$\zeta(s) = k_{\zeta}e^{-2s/p}. \quad (47)$$

Through the inverse time-scale transformation from virtual time to actual time for the controller τ_s with (34) and (36), the feedback control law τ_t in actual time is derived as

$$\tau_t = -\left(a(t)K_3^{-1} - \frac{\dot{a}(t)}{a(t)}\right)\dot{q} - k_{\zeta}\xi^2(t)a^2(t)K_3^{-1}\frac{\partial Q}{\partial q} \quad (48)$$

where k_{ζ} is a positive constant. From (32) and (48), the following feedback controller τ^{ψ} can be derived as

$$\tau^{\psi} = M(q)\tau_t + h(q, \dot{q}) + g(q). \quad (49)$$

When the joint torque τ^{ψ} (49) is selected as τ^* in (28), the joint torque τ_{joint} to control the internal joint motion of the redundant manipulator can be computed.

The total feedback control law τ (29) composed of the designed controllers given in (41) and (49) can lead the end-effector to the target position at the specified time t_f and may attain the desired posture by utilizing the redundancy of the manipulator effectively without altering the configuration of the end-effector.

C. Computer Simulations

The proposed trajectory generation method is applied to a redundant manipulator with the TBG given in (6). Fig. 6 shows the simulation results with a three-joint-planar manipulator. The initial posture of the manipulator is $q(0) = [\pi, -11\pi/12, -\pi/3]^T$ [rad] and the target position of the end-effector is $x^* = [0.0, 1.5]^T$ [m] with the convergence time $t_f = 5.0$ [s] under $p = 8.0$, $\alpha = 1.0$ and the gain $k_{\zeta} = 1.0$. The gain matrices $K_i (i = 1, 2, 3)$ in the potential functions are set as $K_1 = \text{diag.}(0.25, 0.25)$, $K_2 = \text{diag.}(1.0, 1.0)$ and $K_3 = \text{diag.}(1.0, 1.0, 1.0)$, respectively. The computer simulations were executed with the Appel method for the manipulator dynamics [27] and the link parameters of the manipulator as shown in Table I.

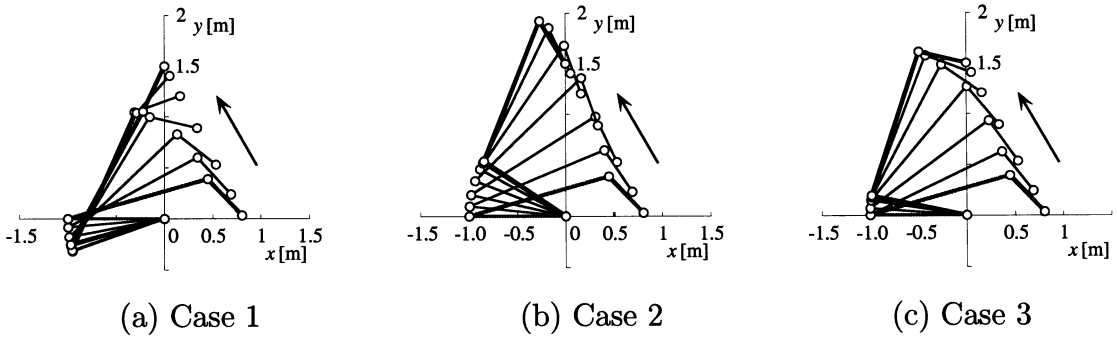

Fig. 6. Motion profiles of the three-joint planar manipulator generating trajectory with the different positive functions $Q_i(q)$ $(i = 1, 2, 3)$.

TABLE I
LINK PARAMETERS OF A THREE-JOINT PLANAR MANIPULATOR

	link 1	link 2	link 3
length [m]	1.0	1.5	0.5
mass [kg]	0.8	1.2	0.4
center of mass [m]	0.4	0.6	0.25
moment of inertia [kgm^2]	0.06666	0.22500	0.00833

Fig. 6(a) shows the generated trajectory with the potential function $Q(q)$ set at

$$Q_1(q) = 0 \tag{50}$$

which means that arm redundancy is not utilized. On the other hand, the joint angle control of the first joint and the maximization of the manipulability [24] are considered as a subtask in Fig. 6(b) and (c), respectively. In these cases, the potential functions $Q(q)$ are given as

$$Q_2(q) = \frac{1}{2}\left(q_1^* - q_1(t)\right)^2 \tag{51}$$

$$Q_3(q) = \sqrt{\det JJ^T} \tag{52}$$

where the target angle of the first joint q_1^* is specified as $q_1^* = 5\pi/6$ [rad]. For the maximization of $Q_3(q)$, we use the negative nondecreasing function $\zeta(s)$

$$\zeta(s) = -k_\zeta e^{-2s/p} \tag{53}$$

instead of (47). It can be seen that the generated trajectories are influenced by the corresponding potential functions $Q(q)$ defined above. Also, the third joint of the manipulator is outstretched while the end-effector reaches the target position in Fig. 6(a). In contrast, the end-effector reaches the target position without any singular configurations by utilizing the redundancy control of the manipulator corresponding to local optimization of the potential functions $Q(q)$ in Fig. 6(b) and (c). Fig. 7 shows the time histories of $Q_2(q)$ and $Q_3(q)$. It can be seen that each potential function in Fig. 6(b) and (c) is optimized much better than other cases, respectively.

Fig. 8 shows the time history of the end-effector position x, velocity $\dot{x}$ and the squared sum of the joint angular velocity. It should be noticed that all generated trajectories of the end-effector in Fig. 6 completely coincide with the one depicted in Fig. 8(a). It can also be observed that the end-effector reached the target position along the smooth trajectory and that the joints

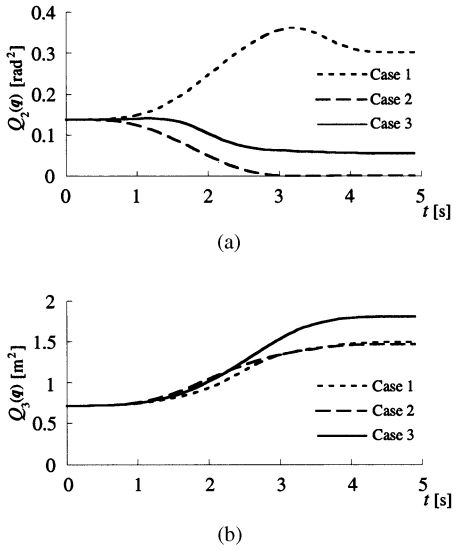

Fig. 7. Time histories of the positive function $Q_i(q)$ $(i = 1, 2, 3)$. (a) Case 2 and (b) Case 3.

of the manipulator did not move any longer after the specified time $t_f = 5.0$ [s] in all cases.

Next, a trajectory generation of a four-link-planar manipulator with link parameters given in Table II is simulated in the polar coordinate task space, where the origin is set at $P = [0.0, 0.4]^T$ [m] [see Fig. 9(a)]. Thus, the task coordinates of the end-effector consist of the angle ϕ between a vector from the point P to the current end-effector's position and the distance r between P and the current position of the end-effector. The initial conditions of the manipulator are $x(0) = [0\,[\text{rad}], 0.2\,[\text{m}]]^T$ and $q(0) = [0, \pi/6, \pi/3, \pi/3]^T$ [rad]. Also, the target position of the end-effector is set at $x^* = [2\pi\,[\text{rad}], 0.2\,[\text{m}]]^T$ with the specified convergence time $t_f = 5.0$ [s].

Fig. 9 shows the generated spatio-temporal trajectories with maximization of the manipulability $Q_3(q)$ defined by (52) under the gain matrices $K_1 = \text{diag.}(0.25, 0.25)$, $K_2 = \text{diag.}(1.0, 1.0)$, $K_3 = \text{diag.}(1.0, 1.0, 1.0, 1.0)$. It can be seen that the circular spatio-trajectory (dotted line) is generated without any singular configurations and the joints do not move after the specified time $t_f = 5.0$ [s].

V. TRAJECTORY GENERATION OF A UNICYCLE-LIKE VEHICLE

Control of a mobile robot with nonholonomic constraints has received a great deal of attention [28]. For closed loop control

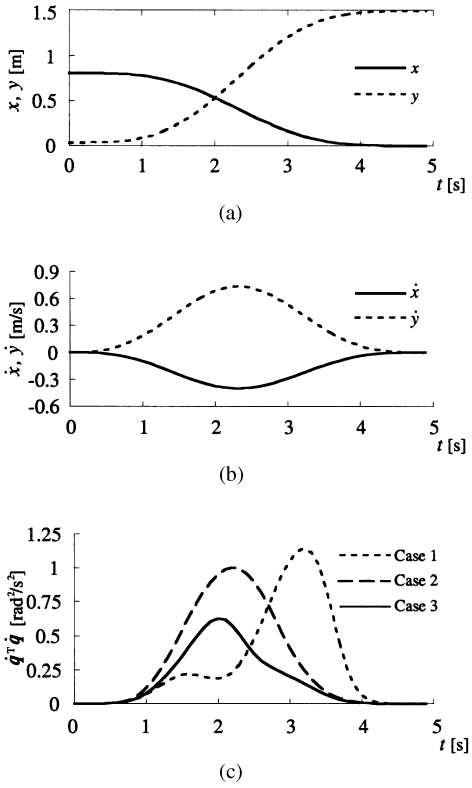

Fig. 8. Dynamic behavior of the manipulator generating trajectory: (a) end-effector position, (b) end-effector velocity, and (c) squared sum of joint velocities.

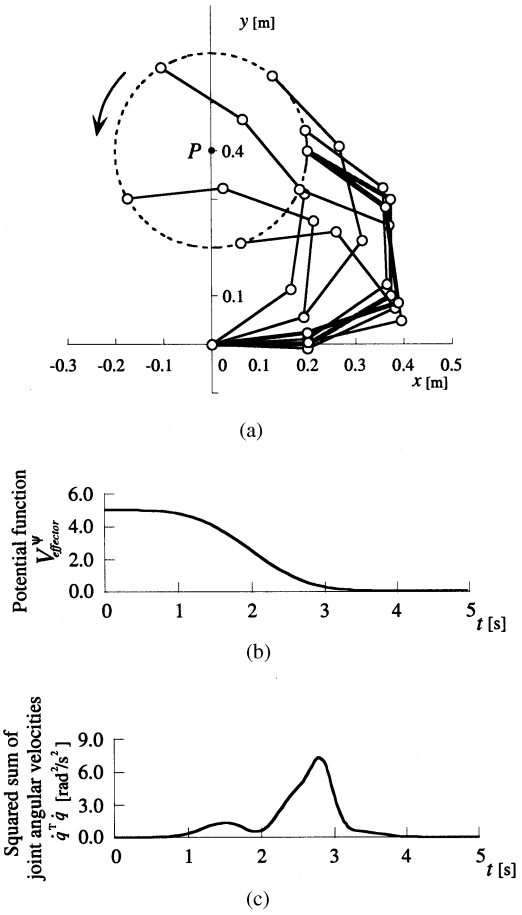

Fig. 9. Motion profile of the four-joint planar manipulator generating trajectory in the polar coordinates: (a) stick pictures, (b) potential function, and (c) squared sum of joint velocities.

on the basis of a kinematic model of a mobile robot, Samson [29] and Pomet [30] proposed a feedback law using periodic time functions and showed that a mobile robot with two driving wheels can be positioned at the given final configuration for any initial condition. Although the smooth time-varying feedback of this approach can assure the stability of the system, slow convergence is a practical defect. Then, Canudas de Wit and Sørdalen [31] proposed a piecewise smooth feedback law using a discontinuous controller and proved the exponential stabilization of the mobile robot. Also, Badreddin and Mansour [32] showed that a special selection of the polar coordinate system representing the position and orientation of the mobile robot allows us to derive a smooth stabilizing control law without contradicting the well known work of Brockett [33]. Casalino *et al.* [34] derived the effective closed loop control law in the framework of the Lyapunov stability theory, which can assure the global stability. In this section, the trajectory generation method using the TBG is applied to a unicycle-like vehicle, that is a mobile robot with two driving wheels.

TABLE II
LINK PARAMETERS OF A FOUR-JOINT PLANAR MANIPULATOR

	link i (i = 1,...,4)
length [m]	0.2
mass [kg]	1.57
center of mass [m]	0.1
moment of inertia [kgm^2]	0.8

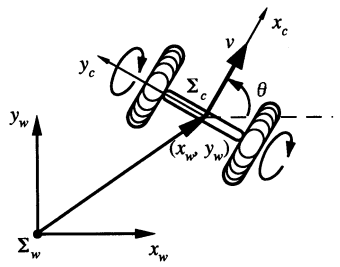

Fig. 10. Unicycle-like vehicle.

A. Model of a Unicycle-Like Vehicle

Fig. 10 shows a unicycle-like vehicle, where Σ_w denotes the world coordinate system (for a planar task space) and Σ_c the moving coordinate system fixed to the vehicle with the origin of Σ_c set between two wheels and x_c axis oriented as the direction of motion of the vehicle. Thus, we can choose the following generalized coordinates of the vehicle: position (x_w, y_w) and orientation angle θ of Σ_c with respect to Σ_w.

The kinematics of the vehicle can be described by the following relationship between the time derivative of the generalized coordinate vector $x = [x_w, y_w, \theta]^T$ and the linear and the angular velocities of the vehicle $u = [v, \omega]^T$:

$$\dot{x} = G(x)u \tag{54}$$

where

$$G(x) = \begin{bmatrix} \cos\theta & 0 \\ \sin\theta & 0 \\ 0 & 1 \end{bmatrix} \tag{55}$$

and the following kinematic constraint must be satisfied [it can be easily derived from (54)]:

$$\dot{x}_w \sin\theta - \dot{y}_w \cos\theta = 0. \tag{56}$$

B. Derivation of the Control Law

Our purpose is to derive a control law that automatically drives the vehicle from the initial configuration to the target configuration. Without any loss of generality, the origin of the world coordinate system Σ_w can be set at the target position, with the x_w axis directed as the desired final orientation of the vehicle (see Fig. 11).

The piecewise smooth feedback control law proposed by Canudas de Wit and Sørdalen [31] uses the family of circles that pass through the origin and the current position of the vehicle and contacts with the x_w axis at the origin as shown in Fig. 11. In the figure, θ_d represents the tangential direction of this circle at the position x belonging to $[-\pi, \pi)$. Their control law is based on the idea that the arc length from the origin to the current position should be decreasing and the current angular orientation of the vehicle should agree with the tangential direction θ_d. In our approach the distance r from the current position to the origin is used instead of the arc length.

Let α denote the angle between the tangential direction θ_d and the current angular orientation θ with the intention of designing a control law which can eliminate this kind of *orientation error* together with the corresponding *positional error* from the target denoted by the distance r. The following coordinate transformation from $x = [x_w, y_w, \theta]^T$ to $z = [r, \alpha]^T$ is then introduced [31]:

$$r(x_w, y_w) = \sqrt{{x_w}^2 + {y_w}^2} \tag{57}$$

$$\alpha(x_w, y_w, \theta) = e + 2n(e)\pi \tag{58}$$

where

$$e = \theta - \theta_d \tag{59}$$

$$\theta_d = 2\arctan 2(y_w, x_w) \tag{60}$$

and $n(e)$ is a function that takes an integer in order to satisfy $\alpha \in [-\pi, \pi)$. Also, $atan2(\cdot,\cdot)$ is the scalar function defined as $atan2(a, b) = \arg(b + ja)$, where j denotes the imaginary unit and $\arg$ denotes an argument of a complex number. As a result, the current state of the vehicle can be represented by

$$z = F(x) = \begin{bmatrix} r(x_w, y_w) \\ \alpha(x_w, y_w, \theta) \end{bmatrix} \tag{61}$$

and the target configuration of the vehicle is transformed to $z_f = [0, 0]^T$. As a result of such coordinate transformation $z = F(x)$, the target configuration of the vehicle can be expressed as $z_f = [0, 0]^T$.

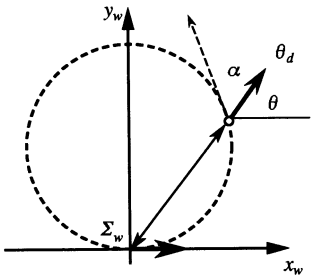

Fig. 11. Coordinate transformation.

In order to derive the control law which can stabilize the system to the target, we can write, first, the relationship between dz/dt and dx/dt

$$\frac{dz}{dt} = \frac{\partial F(x)}{\partial x}\frac{dx}{dt} = J(x)\frac{dx}{dt} \tag{62}$$

where

$$J(x) = \begin{bmatrix} x_w\left({x_w}^2 + {y_w}^2\right)^{-1/2} & y_w\left({x_w}^2 + {y_w}^2\right)^{-1/2} & 0 \\ 2y_w\left({x_w}^2 + {y_w}^2\right)^{-1} & -2x_w\left({x_w}^2 + {y_w}^2\right)^{-1} & 1 \end{bmatrix}.$$

Substituting (54) into (62), we have the relationship between dz/dt and the system input u

$$\frac{dz}{dt} = J(x)G(x)u = B(x)u \tag{63}$$

where

$$B(x) = \begin{bmatrix} b_1 & 0 \\ b_2 & 1 \end{bmatrix} \tag{64}$$

$$b_1(x) = \left({x_w}^2 + {y_w}^2\right)^{-1/2}(x_w\cos\theta + y_w\sin\theta) \tag{65}$$

$$b_2(x) = 2\left({x_w}^2 + {y_w}^2\right)^{-1}(y_w\cos\theta - x_w\sin\theta). \tag{66}$$

It can be found that the number of state variables is reduced to the same number as the system input.

Then, by the time scale transformation for the derived system given in (63), the system can be rewritten in the virtual time scale s as follows:

$$\frac{dz}{ds} = \frac{dz}{dt}\frac{dt}{ds} = B(x)\,u_s \tag{67}$$

where

$$u_s = \frac{1}{a(t)}u. \tag{68}$$

For this time scaled system, the following potential function can be defined:

$$V = \frac{1}{2}z^T\begin{bmatrix} k_r & 0 \\ 0 & k_\alpha \end{bmatrix}z \tag{69}$$

where k_r and k_α are positive constants.

By designing the feedback control law u_s based on the potential function V as

$$u_s = -\frac{1}{2}B(x)^{-1}z \tag{70}$$

the time-derivative of V in the new time scale yields

$$\frac{d}{ds}V = -V \leq 0. \tag{71}$$

Through the inverse time-scale transformation from virtual time s to actual time t for the designed feedback controller u_s with APFA, we can derive the following control law for the original system (63)

$$u = -\frac{1}{2}a(t)B^{-1}(x)z = \begin{bmatrix} \frac{pr\dot{\xi}}{2b_1\xi} \\ -b_2\, v + \frac{p\alpha\dot{\xi}}{2\xi} \end{bmatrix} \tag{72}$$

under the assumption of $\det B(x) \neq 0$ except at the target position.

Substituting the control law (72) into the system (63) yields

$$\frac{dr}{dt} = b_1 v = \frac{pr\dot{\xi}}{2\xi} \tag{73}$$

$$\frac{d\alpha}{dt} = b_2 v + \omega = \frac{p\alpha\dot{\xi}}{2\xi}. \tag{74}$$

Solving the above differential equations, the dynamic behavior of the system state can be given by

$$r = r_0\xi^{p/2} \tag{75}$$

$$\alpha = \alpha_0\xi^{p/2} \tag{76}$$

where r_0 and α_0 are the initial values of r and α, respectively. It can be seen that the *distance error* r and the *angular error* α decrease by the $(p/2)$th power of ξ under the control law (72).

Moreover, the time derivation of the potential function $\dot{V}$ with the derived feedback controller (72) in the actual time scale yields

$$\frac{dV}{dt} = pV\frac{\dot{\xi}}{\xi}. \tag{77}$$

Solving the above differential equation with respect to ξ, V can be represented with the TBG ξ as

$$V = V_0\xi^p \tag{78}$$

where $V_0 = V(x_0)$ is the initial value of V. Thus, it should be noticed that the potential function is "synchronized" with the TBG because V is proportional to the pth power of ξ. Since ξ reaches zero at t_f so must V: in other words, the robot is bound to reach the target position of the vehicle exactly at $t = t_f$.

C. Computer Simulations

1) Generation of Straight Trajectories: First of all, let us consider the case at $x_0 = [x_{w0}, 0, 0]^T$, i.e., the initial position is on the x_w axis and the initial orientation is $\theta_0 = 0\,[\text{rad}]$ as shown in Fig. 12.

In this case, it can be seen from (58)–(60) and the proposed control law (72) that ω is always zero, since $b_2 = 0$ in (66) with $\alpha_0 = 0$. As a result, the vehicle moves in a straight line along x_w axis ($y_w = 0$). Thus yielding $r = \sqrt{x_w{}^2} = |x_w|$, the position of the vehicle is proportional to the $(p/2)$th power of $\xi(t)$

$$|x_w| = |x_{w0}|\,\xi^{p/2}. \tag{79}$$

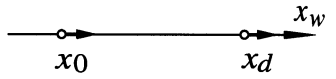

Fig. 12. Generation of a straight trajectory.

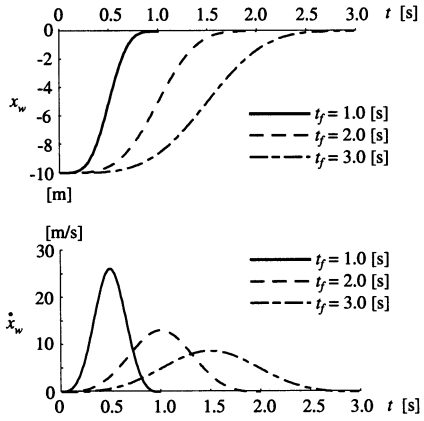

Fig. 13. Straight trajectories with a bell-shaped velocity profile generated by the proposed method of coordinated speed-steering control.

Fig. 13 shows the time histories of x_w and $\dot{x}_w$ generated by the proposed method for the initial position of the vehicle ($x_0 = [-10\ [\text{m}],\ 0\ [\text{m}],\ 0\ [\text{rad}]]^T$) and the bell-shaped velocity TBG defined by (6), where three different convergence times were used ($t_f = 1.0, 2.0, 3.0$ [s]) and the power parameters $p = 2$ and $\beta = 0.75$. It should be noted that the y_w coordinate and the orientation θ of the generated trajectory are always zero. It can be observed that the proposed method can naturally generate a straight path of the vehicle with an easily controllable transient response via the parameters of the TBG.

2) Generation of Curved Trajectories: Figs. 14 and 15 show the results generated by the proposed method of coordinated speed-steering control for several initial conditions located at different points on a circle with a 10 [m] radius: the initial orientation angle θ_0 is $\pi/2$ [rad] in Fig. 14 and 0 [rad] in Fig. 15, respectively. The TBG given in (6) parameters are $t_f = 1.0$ [s], $p = 2$, $\beta = 0.75$.

It can be observed that the control law (72) becomes singular when the term $b_1(x)$ goes to 0. From (65), it is clear that such singularity occurs in the case where the orientation vector of the vehicle is orthogonal with respect to the vector which joins the current to the target position. We tested the property of the control mechanism in the neighborhood of the singular configurations by carrying out a number of simulations with initial conditions very close to singularity. Some of them are included in Figs. 14 and 15: two trajectories starting from locations close to the x_w axis in Fig. 14 ($x_0 = [10\ [\text{m}],\ 1.0 \times 10^{-5}\ [\text{m}],\ \pi/2\ [\text{rad}]]^T$ and $x_0 = [-10\ [\text{m}], -1.0 \times 10^{-5}\ [\text{m}],\ \pi/2\ [\text{rad}]]^T$) and two trajectories starting from points close to the y_w axis in Fig. 15 ($x_0 = [1.0 \times 10^{-5}\ [\text{m}],\ 10\ [\text{m}],\ 0\ [\text{rad}]]^T$ and $x_0 = [-1.0 \times 10^{-5}\ [\text{m}], -10\ [\text{m}],\ 0\ [\text{rad}]]^T$). In all cases, it can be observed that the actual trajectories are repulsed from the singular configuration and the vehicle can arrive at the target position in a smooth way without any forward/backward oscillatory movement.

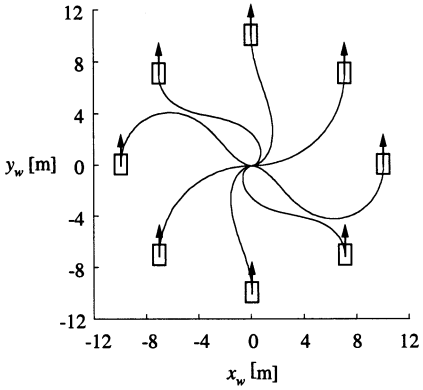

Fig. 14. Trajectories generated by the control law when the vehicle is initially located on a circle in the x_w-y_w plane with $\theta_0 = \pi/2$ [rad]. (The arrow denotes the initial orientation θ_0.).

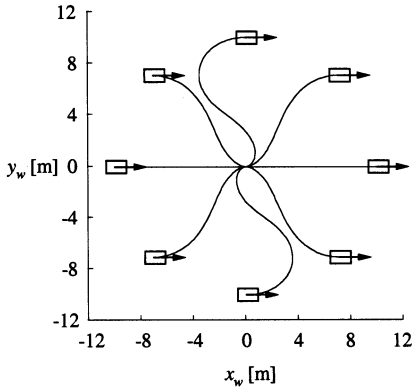

Fig. 15. Trajectories generated by the control law when the vehicle is initially located on a circle in the x_w-y_w plane with $\theta_0 = 0$ [rad]. (The arrow denotes the initial orientation θ_0.).

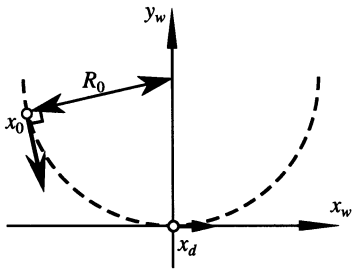

Fig. 16. Generation of a circular trajectory.

3) Regulation of Transient Properties: Let us suppose that the initial orientation θ_0 agrees with the tangential direction of the circle passing through the initial position and the origin as in Fig. 16. From (58) and (72), it can be obtained that $\alpha_0 = 0$ and

$$\omega = -b_2(x)v. \tag{80}$$

Also, the radius of the circle R_0 defined at the initial position can be calculated as

$$R_0 = \frac{{x_{w0}}^2 + {y_{w0}}^2}{2y_{w0}} \tag{81}$$

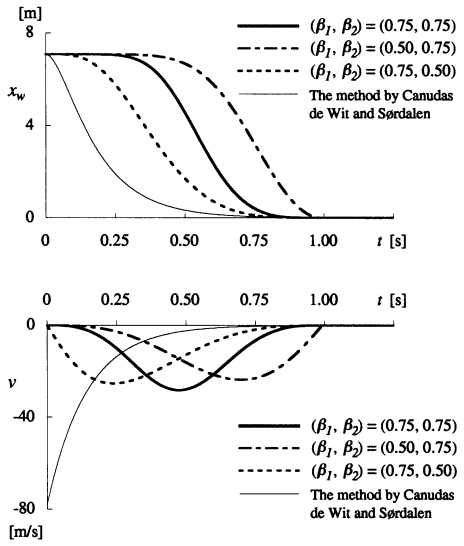

Fig. 17. Regulation of transient behaviors with the different sets of (β_1, β_2) where the initial position of the vehicle is $x_0 = [5\sqrt{2}\ \text{[m]},\ 5\sqrt{2}\ \text{[m]},\ \pi/2\ \text{[rad]}]^T$.

and using simple trigonometric relations ($\sin\theta = x_w/R_0$ and $\cos\theta = (R_0 - y_w)/R_0$) the expression (66) of the gain $b_2(x)$ can be transformed in the following way:

$$b_2 = \frac{2}{{x_w}^2 + {y_w}^2}\left(\frac{R_0 - y_w}{R_0}y_w - \frac{x_w}{R_0}x_w\right) = -\frac{1}{R_0} \tag{82}$$

which indicates that the gain becomes a constant in this situation. As a consequence, the vehicle approaches the target sliding on the circle and reaches it in the planned convergence time.

Here, in such a special case of circular paths, regulation of temporal trajectories is executed by means of the following adjusted TBG as

$$\dot{\xi} = -\gamma\xi^{\beta 1}(1-\xi)^{\beta_2} \tag{83}$$

where $\beta_i\,(i = 1, 2)$ are positive constants under $0 < \beta_i < 1$. When $\beta_1 = \beta_2$, the dynamics reduces to the TBG defined in (6).

Fig. 17 shows the time histories of the x_w coordinate and the linear velocity v with the parameters $(\beta_1, \beta_2) = (0.5, 0.75)$, $(0.75, 0.75)$, $(0.75, 0.5)$ under the initial configuration $x_0 = [5\sqrt{2}\ \text{[m]},\ 5\sqrt{2}\ \text{[m]},\ \pi/2\ \text{[rad]}]^T$. The outputs of the proposed controller are compared with the results of the method by Canudas de Wit and Sørdalen [31] (the fine lines). It can be observed that our method generates the smoother temporal trajectories with the different bell-shaped velocity profiles by changing β_i, which converge to the target in the appointed time t_f, while the latter method tends to approach the target with a progressive slowing down after an initial jerk.

With the change of the parameter p in (12), the dynamic behavior of the robot can be also regulated as shown in Fig. 18, where the initial configuration was set at $x_0 = [5\sqrt{2}\ \text{[m]},\ 5\sqrt{2}\ \text{[m]},\ \pi/2\ \text{[rad]}]^T$. As p is smaller, the robot approaches the target more gradually and peak positions of velocity profiles move to the specified convergence time t_f. On the contrary, as p is larger, the robot moves to the target more quickly.

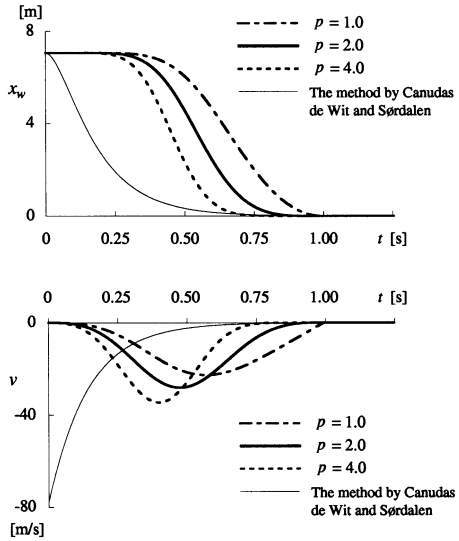

Fig. 18. Regulation of transient behaviors with the change of the parameter p where the initial position of the vehicle is $x_0 = [5\sqrt{2}\ \text{[m]},\ 5\sqrt{2}\ \text{[m]},\ \pi/2\ \text{[rad]}]^T$.

It should be noticed that, in the proposed method, the generating velocity profile of robots can be changed only by adjusting the dynamics of TBG which is made to synchronize with the potential function. Feedback gains in the designed controller and the TBG parameters (β_i, p) are determined with consideration of their influences on the stability and the response of robot motion according to a task space and a given task for the robot. Future research will be directed to establish a way to determine concrete values of the parameters.

4) Response to External Disturbances: At first sight, the proposed method might appear to be a kind of open loop control if we consider that, as the consequence of the control law, the resulting path is described by (75) and (76). However, this is not the case, as it is clearly shown by the simulation illustrated in Fig. 19, in which an external disturbance was applied during movement, suddenly displacing the position of the vehicle: after the vehicle starts from the same initial configuration of Fig. 17, x_w coordinate is externally changed to $x_w = 8$ [m] at time $t = 0.5$ [s]. It should be noted that the large disturbance which may not arise actually is given to the moving robot in order to stress the robustness of the proposed method. It can be seen from the figure that the resulting trajectory, following the disturbance but keeping the same control law, is still able to smoothly converge to the target in the planned time.

In fact, the initial values r_0 and α_0 which appear in (75) and (76) are not computed explicitly in our method but are natural consequences of the feedback control law, which is able to compensate the effect of the external disturbance. Accordingly, even if (75) and (76) are violated by applying the external disturbance, the proportional relationship itself is preserved and the vehicle converges to the target position at the time t_f specified in the TBG.

From the simulation experiments, it can be seen that the designed controller with the proposed method has the robustness for external disturbance under the ideal condition. In the case of controlling a real robot, however, large torque beyond expectations would be generated in order to realize the desired motion

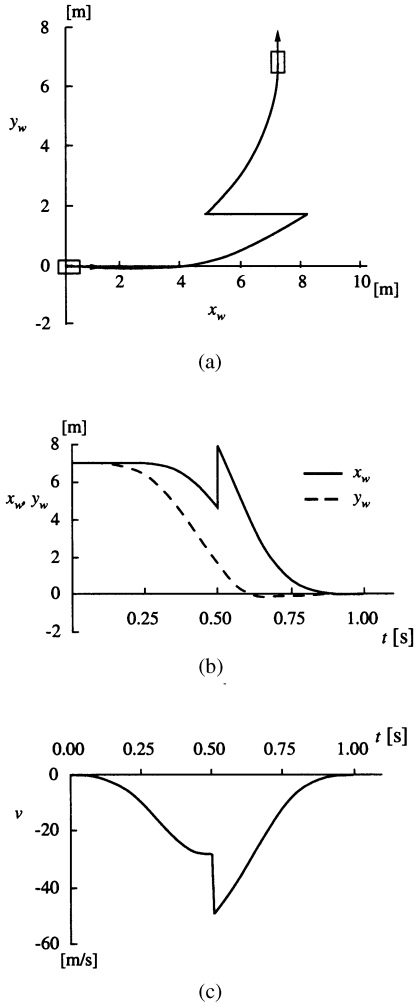

Fig. 19. Generating trajectory when the position of he vehicle is disturbed externally at $t = 0.5$ [s]: (a) spatial trajectory in the x_w-y_w plane, (b) temporal trajectory, and (c) velocity profile.

because of friction and modeling error of the system. It is necessary to carry out experiments with a real robot.

VI. Conclusions

In this paper, the trajectory generation method on the basis of the artificial potential field approach has been proposed. The method has the built-in time function generator called the *Time Base Generator*, defined for a model of human arm movements, by synchronization of the time course of the potential function used as an artificial potential field with the TBG. The method can generate a bio-mimetic trajectory for robots with a bell-shaped velocity profile, which is the minimum jerk trajectory as Flash and Horgan [35] have proposed and can regulate the transient response such as the movement time and the velocity profile of the generating trajectory.

Then, the method was applied to the trajectory generation problem of the redundant manipulator and the unicycle-like vehicle. It was shown that the proposed method matches other control strategies such as the utilization of the arm redundancy and the piecewise smooth feedback law for the nonholonomic vehicle. Also, it had been already shown that the method using

TBG is effective for the obstacle avoidance problem [18], [19] as the previous methods [3]–[13].

The method proposed here can be utilize for coordination of multiple robots since it can regulate the temporal trajectory as well as the spatial trajectory of the robots. Future research will be directed to develop an algorithm of parameter adjustment with consideration of the torque limited problem and to analyze robustness of the proposed feedback controller against disturbances including experiments with a real robot.

APPENDIX A
CONDITION OF THE SYSTEM CONVERGENCY

Solving the derived nonlinear differential (23) with respect to each component of the system variable x_i $(i = 1, \ldots, n)$, the dynamic behavior of x_i is represented according to the discriminant of the characteristic polynomial of (23) $D_{x_i} = 4(k_i/k_{n+i}) - 1$ as follows.

A) if $D_{x_i} > 0$

$$x_i = {}^0x_i \left\{ \cos\left(f(\xi)\right) - \frac{1}{\sqrt{D_x}} \sin\left(f(\xi)\right) \right\} \xi^{p/2}$$
$$f(\xi) = \frac{\sqrt{D_{x_i}}}{2} p \ln \xi. \tag{A-1}$$

B) if $D_{x_i} = 0$

$$x_i = {}^0x_i \left(1 - \frac{p}{2} \ln \xi\right) \xi^{p/2}. \tag{A-2}$$

C) if $-1 < D_{x_i} < 0$

$$x_i = \frac{{}^0x_i}{\lambda_2 - \lambda_1} \left(\lambda_2 \xi^{\lambda_1} - \lambda_1 \xi^{\lambda_2}\right)$$
$$\lambda_1 = \frac{p}{2} + \frac{j\sqrt{D_{x_i}}}{2} p,\ \lambda_2 = \frac{p}{2} - \frac{j\sqrt{D_{x_i}}}{2} p. \tag{A-3}$$

${}^0x_i$ is an initial value of x_i and $j^2 = -1$. Taking account of the definition that $\xi \to 0$ as $t \to t_f$, the following necessary and sufficient condition to bound $x, \dot{x}$ and $\ddot{x}$ at the convergence time t_f can be obtained depending on D_{x_i} as follows:

1) if $D_{x_i} \geq 0$ then $\mathrm{p} > 4(1 - \beta)$;
2) if $-1 < D_{x_i} < 0$ then $\mathrm{p} > 4(1 - \beta)/(1 - j\sqrt{D_{x_i}})$.

APPENDIX B
DYNAMIC BEHAVIOR OF THE POTENTIAL FUNCTION V_Ψ

The time-derivative of the potential function for the new system V_Ψ in the actual time scale yields

$$\frac{d}{dt} V_\Psi = -\frac{1}{a(t)} X^T K_c X = -\sum_{i=1}^{n} \frac{k_{n+i}}{a(t)} \dot{x}_i^2 \leq 0. \tag{B-1}$$

With differentiating and substituting (A-1), (A-2) and (A-3) into (B-1), the potential function for each of component variables V_{ψ_i} can be derived according to D_{x_i} as follows:

A) if $D_{x_i} > 0$

$$V_{\psi_i} = 2C_i \left(\frac{1 + D_{x_i}}{D_{x_i}}\right) \cdot \left\{1 + D_{x_i} - \cos(2f(\xi)) - \sqrt{D_{x_i}} \sin(2f(\xi))\right\} \xi^p \tag{B-2}$$

B) if $D_{x_i} = 0$

$$V_{\psi_i} = C_i \left\{2 - 2p \ln \xi + (p \ln \xi)^2\right\} \xi^p; \tag{B-3}$$

C) if $-1 < D_{x_i} < 0$

$$V_{\psi_i} = C_i \left(\frac{1 + D_{x_i}}{j\sqrt{D_{x_i}}}\right)^2 \left(\frac{2\lambda_1}{p} \xi^{2\lambda_1} + \frac{2\lambda_2}{p} \xi^{2\lambda_2} - 2\right) \tag{B-4}$$

where $C_i = k_{n+i}/16({}^0x_i)^2$. It should be noticed that the potential function V_{Ψ_i} is composed of ξ (TBG) in all cases. Thus, the dynamic behavior of V_{ψ_i} is directed by the TBG to converge toward zero at the specified time t_f under the conditions with respect to the parameter p since $\lim_{t \to t_f} \xi = 0$ and also $\lim_{t \to t_f} \xi \ln \xi = 0$.

REFERENCES

[1] S. Hashimoto *et al.*, "Humanoid robot-development of an information assistant robot hadaly-," in *Proc. 8th IEEE Int. Workshop on Robot and Human Communication*, 1997, pp. 106–111.

[2] K. Hirai, M. Hirose, Y. Haikawa, and T. Takenaka, "The development of Honda humanoid robot," in *Proc. 1998 IEEE Int. Conf. Robotics and Automation*, 1998, pp. 1321–1326.

[3] L. A. Loeff and A. H. Soni, "An algorithm for computer guidance of a manipulator in between obstacles," *Trans. ASME J. Eng. Ind.*, vol. 97, no. 3, pp. 836–842, 1975.

[4] O. Khatib, "Real-time obstacle avoidance for manipulators and mobile robots," *Int. J. Robot. Res.*, vol. 5, no. 1, pp. 90–98, 1986.

[5] C. I. Connolly, J. B. Burns, and R. Weiss, "Path planning using Laplace's equation," in *Proc. 1990 IEEE Int. Conf. Robotics and Automation*, 1990, pp. 2102–2106.

[6] J. O. Kim and K. Khosla, "Real-time obstacle avoidance using harmonic potential functions," *IEEE Trans. Robot. Automat.*, vol. 8, pp. 338–349, June 1992.

[7] K. Sato, "Global motion planning using a laplacian potential field" (in Japanese), *J. Robot. Soc. Jpn.*, vol. 11, no. 5, pp. 702–709, July 1993.

[8] H. Hashimoto, Y. Kunii, F. Harashima, V. I. Utkin, and S. V. Drakunov, "Obstacle avoidance control of multi-degree-of-freedom manipulator using electrostatic potential field and sliding mode" (in Japanese), *J. Robot. Soc. Jpn.*, vol. 11, no. 8, pp. 1220–1228, Nov. 1993.

[9] A. Mohri, X. D. Yang, and M. Yamamoto, "Collision free trajectory planning for manipulator using potential function," in *Proc. 1995 IEEE Int. Conf. Robotics and Automation*, 1995, pp. 3069–3074.

[10] S. Sundar and Z. Shiller, "Time-optimal obstacle avoidance," in *Proc. 1995 IEEE Int. Conf. Robotics and Automation*, 1995, pp. 3075–3080.

[11] ——, "Optimal obstacle avoidance based on the Hamilton-Jacobi-Bellman equation," *IEEE Trans. Robot. Automat.*, vol. 13, pp. 305–310, Apr. 1997.

[12] C. I. Connolly, "Harmonic functions and collision probabilities," *Int. J. Robot. Res.*, vol. 16, no. 4, pp. 497–507, Aug. 1997.

[13] N. V. Dounskaia, "Artificial potential method for control of constrained robot motion," *IEEE Trans. Syst., Man, Cybern. B*, vol. 28, pp. 447–453, June 1998.

[14] P. G. Morasso, V. Sanguineti, and T. Tsuji, "A dynamical model for the generator of curved trajectories," in *Proc. Int. Conf. Artificial Neural Networks*, 1993, pp. 115–118.

[15] ——, "A model for the generator of target signals in trajectory formation," in *Advances in Handwriting And Drawing: A Multidisciplinary Approach*, Faure, Kuess, Lorette, and Vinter, Eds. Europia, Paris, 1994, pp. 333–348.

[16] T. Tsuji, P. Morasso, T. Yamanaka, and M. Kaneko, "Feedback control of mobile robots with nonholonomic constraints using time base generator" (in Japanese), *J. Robot. Soc. Jpn.*, vol. 12, no. 7, pp. 1072–1078, Oct. 1994.

[17] T. Tsuji, P. Morasso, and M. Kaneko, "Feedback control of nonholonomic mobile robots using time base generator," in *Proc. 1995 IEEE Int. Conf. Robotics and Automation*, 1995, pp. 1385–1390.

[18] T. Tsuji, P. Morasso, K. Shigehashi, and M. Kaneko, "Motion planning for manipulators using artificial potential field approach that can adjust convergence time of generated arm trajectory" (in Japanese), *J. Robot. Soc. Jpn.*, vol. 13, no. 2, pp. 285–290, Mar. 1995.

[19] T. Tsuji, K. Chigusa, and M. Kaneko, "Trajectory generation of moving robots using active deformation of artificial potential fields" (in Japanese), *Trans. Jpn. Soc. Mech. Eng.*, pt. C, vol. 62, no. 597, pp. 257–263, May 1996.
[20] M. Zak, "Terminal attractors for addressable memory in neural networks," *Phys. Lett. A*, vol. 133, pp. 218–222, 1988.
[21] M. Sampei and K. Furuta, "On time scaling for nonlinear systems: Application to linearization," *IEEE Trans. Automat. Contr.*, vol. AC-31, pp. 459–462, May 1986.
[22] A. Liegeois, "Automatic supervisory control of the configuration and behavior of multibody mechanisms," *IEEE Trans. Syst., Man, Cybern.*, vol. SMC-7, pp. 868–871, Dec. 1977.
[23] Y. Nakamura, H. Hanafusa, and T. Yoshikawa, "Task-priority based redundancy control of robot manipulators," *Int. J. Robot. Res.*, vol. 6, no. 2, pp. 3–15, 1987.
[24] T. Yoshikawa, "Analysis and control of robot manipulators with redundancy," in *Proc. Robotics Research Int. Symp.*, M. Brady and R. Paul, Eds., Cambridge, MA, 1984, pp. 735–747.
[25] M. Takagi and S. Arimoto, "A new feedback method for dynamic control of manipulators," *Trans. ASME J. Dyn. Sys., Meas., Contr.*, vol. 103, pp. 119–125, June 1981.
[26] O. Khatib, "Motion/force redundancy of manipulators," in *Proc. USA Symp. Flexible Automation*, vol. 1, 1990, pp. 337–342.
[27] V. Potkonjak and M. Vukobratovic, "Two new methods for computer forming of dynamic equation of active mechanisms," *Mech. Mach. Theory*, vol. 14, no. 3, pp. 189–200, 1979.
[28] Z. Li and J. F. Canny, *Nonholonomic Motion Planning*, Z. Li and J. F. Canny, Eds. Norwell, MA: Kluwer, 1993.
[29] C. Samson, "Velocity and torque feedback control of a nonholonomic cart," *Adv. Robot Contr., Lecture Notes in Control Inform. Sci.*, vol. 162, pp. 125–151, 1991.
[30] J. B. Pomet, "Explicit design of time varying stabilizing feedback laws for a class of controllable systems without drift," *Syst. Contr. Lett.*, vol. 18, pp. 139–145, 1992.
[31] C. C. de Wit and O. J. Sørdalen, "Exponential stabilization of mobile robots with nonholonomic constraints," *IEEE Trans. Automat. Contr.*, vol. 37, pp. 1791–1797, Nov. 1992.
[32] E. Badreddin and R. Mansour, "Fuzzy-tuned state feedback control of a nonholonomic mobile robot," in *IFAC World Congr.*, vol. 6, 1993, pp. 577–580.
[33] R. W. Brockett, "Asymptotic stability and feedback stabilization," in *Differential Geometric Control Theory*, R. W. Brockett, R. S. Millmann, and H. J. Sussmann, Eds. Boston, Birkhauser, 1983, pp. 181–191.
[34] G. Casalino, M. Aicardi, A. Bicchi, and A. Balestrino, "Closed-loop steering for unicycle-like vehicles: A simple Lyapunov like approach," *Proc. 4th IFAC Symp. Robot Control*, pp. 335–342, 1994.
[35] T. Flash and N. Hogan, "The coordination of arm movements: An experimentally confirmed mathematical model," *J. Neurosci.*, vol. 5, no. 7, pp. 1688–1703, July 1985.

Toshio Tsuji (A'88–M'99) was born in Kyoto, Japan, on December 25, 1959. He received the B.E. degree in industrial engineering in 1982, the M.E. degree and Doctor of Engineering degrees in systems engineering in 1985 and 1989, all from Hiroshima University, Japan.

He was a Research Associate from 1985 to 1994, and an Associate Professor from 1994 to 2002, with the Faculty of Engineering, Hiroshima University. He was a Visiting Professor with the University of Genova, Italy, from 1992 to 1993. He is currently a Professor with the Department of Artificial Complex Systems Engineering, Hiroshima University. He has been interested in various aspects of motor control in robot and human movements. His current research interests have focused on the control of EMG-controlled prostheses, and computational neural sciences, in particular, biological motor control.

Dr. Tsuji is a member of the Japan Society of Mechanical Engineers, the Robotics Society of Japan, and the Japanese Society of Instrumentation and Control Engineers.

Yoshiyuki Tanaka was born in Hiroshima, Japan, on September 10, 1971. He received the B.E. degree in computer science and systems engineering from Yamaguchi University, Japan, in 1995, and the M.E. and Doctor of Engineering degrees in information engineering from Hiroshima University in 1997 and 2001, respectively.

During 2001-2002, he was a Research Associate with Faculty of Information Sciences, Hiroshima City University. He is currently a Research Associate of Department of Artificial Complex Systems Engineering, Hiroshima University. His current research interests include human motor control system, and robot motion control with application to neurorehabilitation.

Dr. Tanaka is a member of the Robotics Society of Japan and the Japanese Society of Instrumentation and Control Engineers.

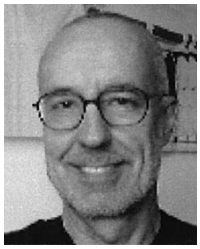

Pietro G. Morasso was born in Genova, Italy, on April 30, 1944. In 1968 he received his Laurea degree in Electronic Engineering cum laude from the University of Genova.

He has been associated with the MIT Department of Psychology, Cambridge, MA, in the Neurophysiological Laboratory of Prof. Emilio Bizzi as a Postdoctoral Fellow (1970–1972), Fullbright Fellow 1973, Visiting Professor 1978–1980. He has had different permanent positions in the Engineering Faculty of the University of Genova since 1970. Currently he is Full Professor of Anthropomorphic Robotics and chairman of the Laurea Programme in Biomedical Engineering. He is Founder and Scientific Director of the Bioiengineering Center at the Rehabilitation Hospital La Colletta in Arenzano since 1995. His scientific interests include the following topics: analysis of the motor control system; computational neuroscience/neuroinformatics; anthropomorphic robotics; rehabilitation engineering. He is author/coauthor of six books, over 300 papers, and two patents (one on robotic navigation and one on laser-therapy).

Vittorio Sanguineti was born in Genova, Italy, in 1964. He got his Master's degree in Electronic Engineering in 1989 and his Ph.D. degree in 1994, both as the University of Genova.

As a post-doctoral fellow, he has been working at the Institut National Polytechnique de Grenoble, France (1995–1996), at McGill University (1996) and at the Northwestern University Medical School (1997–1998), where he returned (1999–2001) as a visiting scientist. Since 1999 he is an Assistant Professor of bioengineering at the Department of Informatics, Systems and Telematics (DIST) of the University of Genova. His research interests include neural control of movements—in particular, the contribution of muscle visco-elasticity in reaching and speech and the role of the cerebellum in sensorimotor control; neural networks and the cellular aspects of sensorimotor learning in vertebrates.

Makoto Kaneko (A'84–M'87–SM'00) received the B.S. degree in mechanical engineering from Kyushu Institute of Technology, Japan, in 1976, and the M.S. and Ph.D. degrees in mechanical engineering from Tokyo University, Japan, in 1978 and 1981, respectively.

From 1981 to 1990, he was a Researcher with the Mechanical Engineering Laboratory, Ministry of International Trade and Industry. From 1988 to 1989, he was a Postdoctoral Fellow with the Technical University of Darmstadt, Germany. From 1990 to 1993, he was an Associate Professor at Kyushu Institute of Technology. Since 1993, he has been with Hiroshima University, as a Professor with the Graduate School of Engineering. His research interests include tactile-based active sensing, grasping strategy, and medical robotics.

Dr. Kaneko received eight academic awards, such as Humboldt Research Award, IEEE ICRA Best Manipulation Award and the IEEE IASTP Outstanding Paper Award. He served as a Technical Editor of IEEE TRANSACTIONS ROBOTICS AND AUTOMATION from 1990 to 1994. He is a member of the RAS, SMC, and IES.